

X-RAY LINE EMISSION FROM THE HOT STELLAR WIND OF θ^1 ORI C

N. S. SCHULZ, C. R. CANIZARES, D. HUENEMOERDER, AND J. C. LEE
 Center for Space Research, Massachusetts Institute of Technology, Cambridge, MA 02139.

accepted for publication in The Astrophysical Journal Letters

ABSTRACT

We present a first emission line analysis of a high resolution X-ray spectrum of the stellar wind of θ^1 Ori C obtained with the High Energy Transmission grating Spectrometer onboard the Chandra X-ray Observatory. The spectra are resolved into a large number of emission lines from H- and He-like O, Ne, Mg, Si, S, Ar and Fe ions. The He-like Fe XXV and Li-like Fe XXIV appear quite strong indicating very hot emitting regions. From H/He flux ratios, as well as from Fe He/Li emission measure ratios we deduce temperatures ranging from 0.5 to 6.1×10^7 K. The He-triplets are very sensitive to density as well. At these temperatures the relative strengths of the intercombination and forbidden lines indicate electron densities well above 10^{12} cm⁻³. The lines appear significantly broadened from which we deduce a mean velocity of 770 km s⁻¹ with a spread between 400 and 2000 km s⁻¹. Along with results of the deduced emission measure we conclude that the X-ray emission could originate in dense and hot regions with a characteristic size of less than 4×10^{10} cm.

Subject headings: stars: early type — X-rays: stars — binaries: stellar winds — techniques: spectroscopic

1. INTRODUCTION

X-ray spectra from stellar winds have been quite difficult to interpret, since the first observations with *Einstein* (Seward et al. 1979). The spectral resolution from previous X-ray missions was insufficient for resolving any emission and absorption lines. Models that describe the mass loss from a hot luminous star successfully in the UV (Pauldrach et al. 1994, Lamers et al. 1999) could never correctly predict observed X-ray fluxes. A model involving a possible hot corona seems unlikely due to the lack evidence for absorption at the 20.6 Å K-shell ionization edge from oxygen (Cassinelli & Swank 1983); additionally no coronal line emission (i.e. Fe XIV at 530 nm) was found in optical spectra of η Ori and κ Ori (Nordsieck et al. 1981) nor in the prototype star for stellar winds ζ Pup (Baade & Lucy 1987). X-ray emission from shocks emerging in instabilities within a radiatively driven wind forming a forward shock was proposed by Lucy & White (1980) and Lucy (1982). However, reverse shocks that decelerate material as it rams into dense shells ahead seem more likely (Owocki et al. 1988). These models predict X-rays up to a temperature of about kT \sim 0.5 keV. Feldmeier et al. (1997) introduced turbulent perturbations into their calculations which ultimately allowed for higher temperatures.

Several recent observations with the 0.1 to 10.0 keV ASCA bandpass, i.e. of τ Sco (Cohen et al. 1997) and η Car (Tsuboi et al. 1997), indicated that there is a hard component to these spectra at > 2 keV. Although these two examples tend to resemble quite extreme cases of massive stars, ASCA observations of other, less massive O-stars (Corcoran et al. 1994), and the Orion Trapezium (Yamauchi et al. 1996) indicated the existence of a similar hard component in their spectra as well. In the most recent analysis of *Chandra* CCD spectra of the Orion Trapezium, Schulz et al. (2000) were able to resolve the entire Trapezium into individual sources. Identified O- and B-stars showed a soft component at ~ 0.8 keV as observed with *ROSAT*; the very early spectral types required an additional hard component of temperatures above 2 keV as well.

In this letter we present first results from an observation of θ^1

Ori C with the High Energy Transmission Grating Spectrometer (HETGS, Canizares et al. 2000, in preparation) onboard *Chandra* (Weisskopf et al. 1996). We present an X-ray line list of the brightest emission lines detected and investigate emission line properties to determine the range of temperatures and densities of the line emitting regions. Some of the results will have immediate impact constraining models of stellar winds.

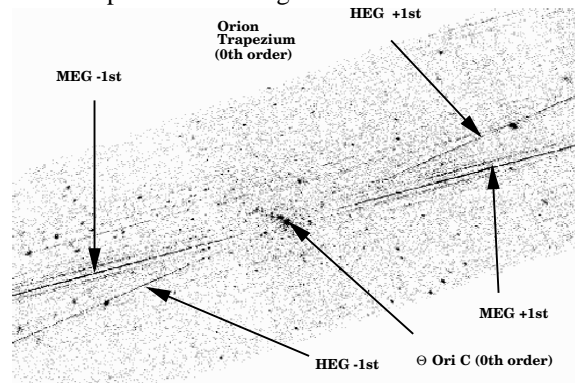


FIG. 1.— HETGS focal plane image of the Orion Trapezium Cluster

2. CHANDRA OBSERVATIONS AND DATA REDUCTION

θ^1 Ori C was observed with the HETGS on 1999 October 31 (05:47:21 UT) continuously for 53 ks. The HETGS carries two different types of transmission gratings, the Medium Energy Gratings (MEG) and the High Energy Gratings (HEG) with grating constants of 4000 and 2000 Å, respectively. It allows for high resolution spectroscopy between 1 and 35 Å with a peak spectral resolution at 12 Å of $\lambda/\Delta\lambda \sim 1400$ and at 1.8 Å of $\lambda/\Delta\lambda \sim 180$ in 1st order HEG. The dispersed spectra were recorded with the Advanced CCD Imaging Spectrometer (Garmire et al. 2000, in preparation). We also refer to the available Chandra X-ray Center (CXC) documents for more detailed descriptions.

We recorded a total of 4.5×10^4 events in the co-added 1st order MEG and 1.7×10^4 events in the HEG after standard grade selection. The level 1 event lists provided by the CXC were re-

processed using the latest available data processing input products. One of the major difficulties in the spectra extraction was that θ^1 Ori C is located in the core of the Orion Trapezium Cluster, which has several sources that are bright enough to produce dispersed spectra as well as many X-ray sources in the vicinity which then would imitate emission lines by coincidence. Most of these contributions can be removed by checking for dislocations of the source point spread functions from the center of the cross-dispersion profile, by cross-correlating with each dispersion arm, and finally by the energy discrimination of the focal plane CCDs.

In order to determine the zero point of the wavelength scale we fitted the dispersed images of the MEG and HEG and determined the intersections of these fits with the zero order read out trace of the CCD. The fits of the MEG and HEG were consistent within 0.3 detector pixels (~ 0.003 Å in MEG and 0.002 Å in HEG 1st order). The current status of the overall wavelength calibration is of the order of 0.1% and mostly depends on uncertainties in the position of CCD gaps (± 0.5 pixels). This leads to a worst case uncertainty in the scale of 0.01 Å in 1st order MEG, 0.008 Å in 1st order HEG, 0.003 Å in 3rd order MEG. Level 1 to 1.5 event list processing as well as aspect corrected exposure map computations were done using available CXC software, the final grating spectra were extracted using custom software and FTOOLS, spectral fits were performed with ISIS.

3. HETGS SPECTRA

Figure 1 shows the focal plane image of the Orion Trapezium Cluster and its dispersed spectra. Several sources in the cluster are bright enough to produce highly resolved grating spectra. The brightest trace in the middle corresponds to θ^1 Ori C; arrows point to its 0th order image as well as the -1st and +1st MEG and HEG spectral trace. The extracted and cleaned spectra are shown in Figure 2. The solid line shows the MEG co-added 1st order spectrum, similarly the dotted line for the HEG. The spectral binning is 0.01 Å. The spectra show a substantial continuum and numerous emission lines. At the current stage of analysis we concentrate on relevant properties of the emission lines; global model fits will be left for subsequent papers.

3.1. Emission Lines

Table 1 displays prominent and for this analysis most interesting set of lines we have identified so far. We observe lines in a band from 1.8 to 19 Å. There is not much flux above 22 Å, since θ^1 Ori C is moderately absorbed with a column density of 1.93×10^{21} cm $^{-2}$ (Schulz et al. 2000). The detected lines are from all major abundant elements, i.e from H-like and He-like ions of O, Ne, Mg, Si, S, and Fe. Calcium and Argon lines are not apparent - they are either missing or below our statistical detection limits. The Lyman- α lines are strongly detected in all other species but Fe. For some ions we also observe the Lyman- β and higher transitions. In 5 ions, S, Si, Mg, Ne, and O, we resolve the He-like triplets into resonance (r), intercombination (i), and forbidden (f) lines. The Ne triplet is contaminated by Fe transitions. The triplet in Fe XXV is not resolved and the line appears considerably broadened. Iron is quite abundant and in addition to many lower transitions, we observe strong lines from He-, Li-, and Be-like Fe. Here we only include Fe XXV and some lines from Fe XXIV and Fe XVII, which we use for plasma diagnostics, a full investigation of the Fe lines is under way.

TABLE 1
EMISSION LINES FROM H- AND HE-LIKE IONS AND FROM SOME FE XXVII AND FE XXIV IONS.

Ion	type	$\lambda(\text{exp.})$ Å	$\lambda(\text{meas.})^1$ Å	Flux 2	Fwhm 10^{-2} Å
Fe XXV	He4	1.851	1.856	7.533	3.07 ⁴
Fe XXIV	Li2	7.987	7.984	2.596	3.17
S XVI	H2	3.990	3.997	1.458	2.31 ⁴
S XVI	H1	4.730	4.729	6.141	1.46
S XV	He4	5.040	5.040	9.457	3.54
S XV	He5	5.060	5.060	2.734	0.13
S XV	He6	5.100	5.105	4.334	2.17
Si XIV	H2	5.220	5.218	3.913	3.34
Si XIV	H1	6.180	6.182	11.742	0.81
Si XIII	He4	6.650	6.650	7.313	1.11
Si XIII	He5	6.690	6.690	4.068	1.64
Si XIII	He6	6.740	6.740	5.579	1.63 ⁴
Mg XII	H2	7.100	7.105	3.218	2.34
Mg XI	He2	7.470	7.466	2.100	2.51
Mg XII	H1	8.420	8.418	8.755	1.38
Mg XI	He4	9.170	9.169	3.000	1.65
Mg XI	He5	9.230	9.237	1.000	0.24
Mg XI	He6	9.310	9.316	0.600	–
Ne X	H4	9.480	9.474	5.834	–
Fe XXIV	Li6A	11.031	11.036	6.255	1.36
Fe XXIV	Li6B	11.184	11.178	5.879	0.35 ⁴
Fe XXIV	Li7B	11.269	11.267	1.539	1.65
Fe XXIV	Li7A	11.445	11.430	2.724	3.16
Ne X	H1	12.130	12.145	12.950	3.47 ⁴
Ne IX	He4	13.440	13.445	2.768	0.71
Fe XVII	Ne4	15.013	15.020	12.424	4.59
O VIII	H2	16.010	16.019	2.441	4.63 ⁴
O VIII	H1	18.970	18.991	9.547	1.39
O VII	He4	21.600	21.600	1.428	0.24
O VII	He5	21.800	21.790	2.452	0.19

¹ in units of 10^{-5} photons cm $^{-2}$ s $^{-1}$

² appear blended

In order to determine line positions, widths and fluxes we treated the underlying continuum as background and performed local fits using a generic flat model for the background and Gaussian functions for the lines. For the line identifications and nomenclature we use the line list presented by Mewe et al. (1985). The wavelength identification is based on the closest known transition within the instrument resolution. Because of its superior resolution line centroids below 13 Å are determined using the HEG. The difference between the measured and expected line positions are well within the current uncertainties of the Chandra wavelength calibration; no obvious systematic shifts other than a trend for larger deviations at higher wavelength exists, which can be explained by the increasing uncertainty due to more CCD gaps in the dispersion direction.

3.2. Velocities

We mostly rely on the a factor 2 superior resolution of the HEG for line width measurements < 13 Å. These widths are shown in column 6 of Table 1. Instrumental corrections have been applied using the latest HETGS response files. The most reliable widths come from the bright and unblended Lyman α lines, where we consider the fine structure splits negligibly small.

The FWHM of the lines range between 0.3 and 4.1×10^{-2} Å, an order of magnitude too large to be interpreted as thermal broadening. If we deduce Doppler velocities from $\Delta\lambda/\lambda = v_D/c$, we obtain a distribution of velocities with a mean value

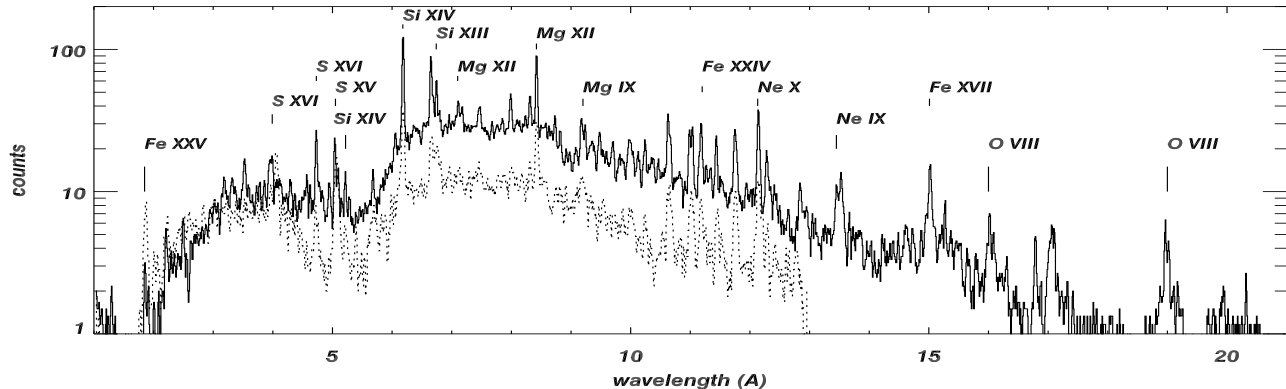


FIG. 2.— The 1st order MEG (solid line) and HEG (dotted line) count spectra

of 771 km s^{-1} (Figure 3). The Fe XXV width at 1.85 \AA appears exceptionally wide, but we do not have the sensitivity to resolve its r, i, and f components. However if we force the fit using the triplet model, we obtain a mean width corresponding to with a velocity of 1650 km s^{-1} . Near 11 \AA we also introduce systematic uncertainties by fitting weak as well as more blended lines adding to an additional scatter in the observed line widths. The drop at 11 \AA , in that respect, may not be real. When we for the time being ignore these weaker data points, the velocity scatter is ~ 400 to 2000 km s^{-1} . We do not observe any measurable asymmetries in the line shapes, which would indicate deviations from an isotropic wind emission geometry.

3.3. Temperatures & Electron Densities

Flux ratios of highly ionized ions are sensitive to the density and temperature of a collisionally ionized plasma (see Mewe 1999 for a review). We have several ways to estimate the local temperature from the line. We can use the (f+i)/r flux ratio of the He-like triplet, flux ratio of the H-like Lyman α to the He-like resonance lines, as well as He- to Li-like and He- to Ne-like ion flux ratios. Comparing the line ratios with theory is difficult and depends on a variety of assumptions. Here we use the Astrophysical Plasma Emission Code (APEC) and the corresponding database (APED¹) described by Smith et al. (1998). In general we make the assumption that for a specific transition the emitting plasma is isothermal or at least has a symmetric distribution with that peak temperature. We also assume that the emitting plasma is in ionization equilibrium. The ratios within the He-like triplets are good indicators for the local plasma temperature. A comparison of the flux ratios to calculated ratios from the database yields temperatures of $4.2 \pm 3.1 \times 10^5 \text{ K}$ for O, $9.3 \pm 3.8 \times 10^6 \text{ K}$ for Mg, $2.0 \pm 1.4 \times 10^6 \text{ K}$ for Si, and $1.5 \pm 1.1 \times 10^7 \text{ K}$ for S. The line flux ratios of the H- to He-like ions as well as the He- to Li-like Fe ions are good indicators of the temperature largely independent of density. Here the ratios for the Lyman α transitions of O, Ne, Mg, Si, and S yields temperatures of 0.6 ± 0.2 , 0.7 ± 0.2 , 1.5 ± 0.2 , 2.0 ± 0.3 , and $2.3 \pm 0.3 \times 10^7 \text{ K}$, respectively. The O, Ne, and Mg ratios have also been corrected for the effect of interstellar column density. Since we do not detect the Lyman α line from Fe, we can only set an upper limit to the temperature of $6.3 \times 10^7 \text{ K}$ by computing the ratio of its 3σ detection limit to the whole detected He-like Fe triplet. This limit is consistent with the

results from the Li-like Fe-lines which predict temperatures between 3.5 and $5.1 \times 10^7 \text{ K}$. From the the ratio with the Ne-like Fe XVII line we deduce a lower temperature of $5.0 \times 10^6 \text{ K}$.

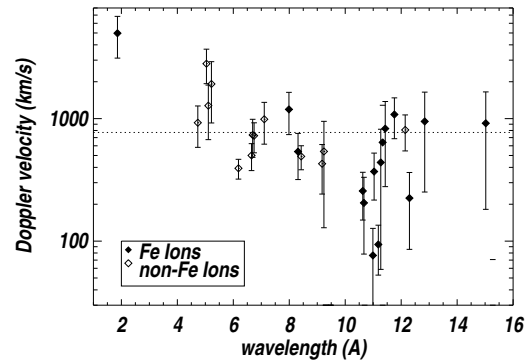


FIG. 3.— Instrument corrected Doppler velocities deduced from fitted line widths. The dotted line shows the mean velocity, the dashed line the instrument width of the HEG.

Although the uncertainties in the (f+i)/r flux ratios are higher, since the ratio uses 3 relatively weak lines, the temperatures for O and Si are significantly lower than the ones deduced from the hydrogenic lines. In the case of Si this in part could be due contamination of the forbidden line with the Mg XII Lyman γ line. However, if we assume that we do not observe the Si XIII forbidden line at all, we deduce a temperature, which is still a factor 2 lower than the one from the hydrogenic lines. The fact that these temperatures are systematically lower could either mean that we are not in ionization equilibrium, or, which we consider more likely, that part of the He-like and lower transitions originate from different, somewhat cooler zones.

The forbidden line intensity in the He-like triplets is metastable and thus density sensitive. However, it should also be noted that this ratio may also be affected by external radiation fields (Kahn et al. 2000). Here we simply compare the f/i ratio to the expectation from emissivity calculations from the APED database. In general, the ratios from elements of higher Z than Si are not suited for this analysis, because here the ratio is not much sensitive to densities below 10^{15} cm^{-3} , which we do not expect here. From the database we deduce a lower density sensitivity limit of the f/i ratio to roughly 10^{10} cm^{-3} for O, 10^{12} cm^{-3} for Mg, and 10^{13} cm^{-3} for Si. For these ions we measure

¹<http://hea-www.harvard.edu/APEC/>

f/i ratios of 0.04 ± 0.02 , 0.60 ± 0.18 , and 1.37 ± 0.51 corresponding to electron densities to $3.5 \pm 2.7 \times 10^{12} \text{ cm}^{-3}$ for oxygen, $4.3 \pm 2.3 \times 10^{13} \text{ cm}^{-3}$ for Mg, and $9.0 \pm 10.6 \times 10^{13} \text{ cm}^{-3}$ for Si. We fixed the temperature to the ones obtained from the hydrogenic lines, because the latter lines are less density sensitive and we also assume that they are not affected by opacity effects. The uncertainties reflect the average upper and lower density limits according to the errors in the ratios. The O-ratio is a lower limit, because as a result of not observing the forbidden line, we estimated the flux based on a 3σ detection limit. We observe a significant flux in the Mg XII Lyman β line, which makes it very likely that the forbidden line in Si at 6.74 \AA is contaminated with a Mg XII Lyman γ line. From the APED database we calculated a emissivity ratio of the Mg XII Lyman β to Lyman γ of 3.05. Based on the observed flux for the Lyman β line we can then estimate the flux contribution of the Mg XII Lyman γ line to the Si XIII forbidden line. The f/i ratio in Si reduces then from 1.37 to 1.11.

Using the lines in Table 1 we also deduced volume emission measures (VEM) assuming isothermal and isotropic conditions. We obtain the lowest VEM from Fe XVII with $1.52 \times 10^{54} \text{ cm}^{-3}$ and the highest from S XVI with $2.5 \times 10^{56} \text{ cm}^{-3}$. If we apply the deduced range of densities above and spherical geometry we find characteristic emission sizes between $4.0 \times 10^8 \text{ cm}$ and $3.9 \times 10^{10} \text{ cm}$.

4. DISCUSSION

A large number of emission lines were detected with a signal to noise ratio of greater than 5σ . These lines are from H- and He-like ion species of Fe, S, Si, Mg, Ne, and O; Ca and Ar are not detected. We do not observe any residual line shifts we could attribute to the source.

The X-ray lines appear significantly broadened implying a mean shock velocity of 770 km s^{-1} . A similar shock velocity of 500 km s^{-1} has been determined from *ROSAT* fits of ζ Pup spectra (Hillier et al. 1993). Within the statistical uncertainties and the current state of the analysis, the line profiles appear symmetric showing blue and red-shifts of equal proportions. We therefore conclude that the wind emission is quite isotropic. Our estimates from the VEM indicates that the emission volume is equivalent to a volume of well within one stellar radius. However, Simulations by Feldmeier et al. (1997) indicated that the X-ray emission must extend far out into the wind. Estimating the distance of the X-ray producing shell collision

we use the β velocity law (with $\beta=0.88$) and a terminal velocity of $\sim 1000 \text{ km s}^{-1}$ (Prinja et al. 1990) to determine the distance where the wind reaches 770 km s^{-1} , which gives about 4 stellar radii. In this respect it is plausible that the X-ray emitting regions appear in very thin dense shells as described by Feldmeier et al. (1997). Their model, however, predicts strong variability of the X-ray emission, which, at least in terms of total X-ray flux, is not observed during our observations.

Whatever the actual emission geometry turns out to be, the emitting regions of θ^1 Ori C appear well confined, hot, and dense with a temperatures ranging between 0.05 and $6 \times 10^7 \text{ K}$ (0.06 to 4.5 keV) and densities above 10^{12} cm^{-3} . CCD spectra of θ^1 Ori C already indicated that the X-ray emission must have a hot component with a temperature of $kT \sim 3 \text{ keV}$ (Yamauchi et al. 1997, Schulz et al. 2000) or equivalent to $\sim 4 \times 10^7 \text{ K}$. A broadband study ranging from UV to ASCA spectra of the B0 V star τ Sco Cohen (1996) also suggested that wide range of temperatures up to 10^7 K is necessary to describe X-ray and UV emission. It is quite hard to explain such high temperature with the line driven shock instability models (Lucy & White 1980, Lucy 1982), which predict temperatures more on the order of $5 \times 10^6 \text{ K}$. The spectrum in Figure 2 also shows that the hard part of the spectrum cannot be explained by inverse Compton scattering of UV photons (Chen & White 1991), since it shows emission lines with similar characteristics than the low energy lines. The approach by Feldmeier et al. (1997) seems to provide promising ingredients to describe the co-existence of low and high temperatures at relatively high densities. A most recent analysis by Kahn et al. (2000) of XMM RGS spectra of ζ Pup also resulted in low f/i line ratios and thus high density values, but it was suggested that a high UV radiation field could destroy the He-like forbidden line leading to an overestimation of the density.

It still remains to be explained whether the high temperatures in θ^1 Ori C and other hot candidates are the exception or the rule. Clearly, we need more high resolution X-ray observations of massive O-Stars in order classify the X-rays in terms of their line emission properties. These properties include temperature ranges, densities, emission volumes and ionization balance.

The authors want to thank N. Brickhouse for providing additional atomic data tables and the Chandra X-ray Center for its enormous support. This research is funded by contracts SV-61010 and NAS8-39073.

REFERENCES

- Baade D., and Lucy L.B., 1987, *A&A* 178, 213
 Cassinelli J.P. and Swank J.H., 1983, *ApJ* 271, 681
 Chen W., and White R.L., 1991, *ApJ* 366, 512
 Chlebowski T., Hamden F.R. jr., and Sciortino S., 1989, *ApJ* 341, 427
 Cohen D.H. 1996, *PASP* 108, 1140
 Cohen D.H., Cassinelli J.P., and Waldron W.L., 1997, *ApJ* 488, 397
 Corcoran M.F., Waldron W.L., MacFarlane J.J., et al., 1994, *ApJ* 436, L95
 Feldmeier A., Kudritzki R.P., Palsa R., Pauldrach A.W., and Puls J., 1997, *A&A* 320, 899
 Feldmeier A., Puls J., and Pauldrach A.W., 1997, *A&A* 322, 878
 Hillier D.J., Kudritzki R.P., Pauldrach A.W., Baade D., Casinelli J.P., Puls J., and Schmitt J.H.M.M., 1993, *A&A* 276, 117
 Pauldrach A.W., Kudritzki R.P., Puls J., Butler K., and Hunsinger J., 1994, *A&A* 283, 525
 Prinja R.K., Barlow M.J., and Howarth I.D., 1990, *ApJ* 361, 607
 Kahn S.M., Leutenegger M., Cottam J., Rauw G., Vreux J.M., den Boggen T., Mewe R., and Guedel M., *A&A* submitted
 Lamers H.J.G.L.M., Haser S., De Koter A., and Leitherer C., 1999, *ApJ* 516, 872
 Lucy L.B., and White R.L., 1980, *ApJ* 241, 300
 Lucy L.B., 1982, *ApJ* 255, 286
 Mewe R., Gronenschild E.H.B.M., and van den Oord G.H.J., 1985, *A&ASuppl.* 62, 197
 Mewe R., 1999, *Atomic Physics of Hot Plasmas*, in "X-ray Spectroscopy in Astrophysics", eds. J. van Paradijs and J.A.M. Bleeker, Springer-Verlag, p.109
 Nordsieck K.H., Cassinelli J.P., and Anderson C.M., 1981, *A&A* 248, 678
 Owocki S.P., Castor J.I., and Rybicki G.B., 1988, *ApJ* 335, 914
 Schulz N.S., Canizares R.C., Huenemoerder D., Kastner J., and Taylor S., 2000, *ApJ* submitted
 Seward F.D., Froman W.R., Giacconi R., Griffith R.E., Hamden F.R. jr., Jones C., Pye J.P., 1979, *ApJ* 234, 55
 Smith R.K., Brickhouse N.S., Raymond J.C., and Liedahl D.A., 1998, in *Proceedings of the First XMM Workshop on "Science with XMM"*, Noordwijk, The Netherlands: ESA
 Tsuboi Y., Koyama K., Sakano M., and Petre R., 1997, *PASJ* 49, 85
 Weisskopf M.C., O'Dell S.L., and van Speybroeck L.P., 1996, *Proc. SPIE* 2805, 2
 Yamauchi S., Koyama K., Sakano M., and Okada K., 1996, *PASJ* 48, 719